Restoration of Color Images by Multichannel Kalman Filtering

Nikolas P. Galatsanos, *Member, IEEE,* and Roland T. Chin, *Member, IEEE*

Abstract—**A multichannel image is a set of image planes that exhibit between-plane correlations. Degradation of multichannel imagery involves both within- and between-channel blurs. Restoration of such images using existing independent-channel filters is not appropriate because they fail both to restore the between-channel degradation and to incorporate between-channel correlations in the process. In this paper, a Kalman filter for optimal restoration of multichannel images is presented. This filter is derived using a multichannel semicausal image model that includes between-channel correlation and an imaging equation with between-channel degradation. Both stationary and nonstationary image models are developed. This filter is implemented in the Fourier domain and computation is reduced from $O(\Lambda^3 N^3 M^4)$ to $O(\Lambda^3 N^3 M^2)$ for an $M \times M$ N-channel image with degradation length Λ. Color (red, green, and blue (RGB)) images are used as examples of multichannel images, and restoration in the RGB and YIQ domains are investigated. Simulations are presented in which the effectiveness of this filter is tested for different types of degradation and different image model estimates.**

I. Introduction

IMAGE restoration is often performed on images to remove degradation and noise for subsequent human or machine analysis. In the past twenty years many researchers have addressed the problem of single-channel image restoration. Recently, the research effort in this area has been concentrated on simultaneous identification of blur and restoration, and on multichannel processing, see [6], [11], [12], [17], [8], and [4].

In this paper we consider the problem of restoring multichannel imagery, which is a set of image planes (channels) acquired by an imaging system that measures the same scene using more than one sensor. Examples of multichannel images include multispectral satellite images, color images, multiple time frames, and multiple sensor images; all of these display signal interdependency among channels. Degradation in these imaging systems may involve both spatial and between-channel blurring. Examples of between-channel degradations include channel crosstalks, leakage in detectors, and spectral blurs.

In contrast to single-channel processing, multichannel restoration has received little attention from the research community and is still in its infancy. The extension of existing single-channel image restoration techniques to multichannel restoration is a nontrivial task, mainly because of the lack of multichannel image processing theories and of computational algorithms for multiple images. Furthermore, filters that are optimal for single-channel images may be suboptimal when applied individually to the separate channels of a multichannel image.

Hunt and Kübler in [8] formulated a multichannel Wiener restoration filter which minimizes the mean-square error (MMSE) between the ideal and the restored image. It uses both the between-channel and the within-channel correlation and assumes that the signal autocorrelation describing the between-channel and within-channel relationship is separable. This enables the formulation of the Karhunen–Loeve transformation to decorrelate the signal between image channels, making the channels orthogonal. It follows that multichannel restoration of the transformed signal under this assumption is equivalent to the independent restoration of individual channels, and the process does incorporate between-channel information. Therefore, subsequent filtering of individual channels can be done by conventional single-channel image restoration algorithms. However, the use of the separable assumption in practical images is considered restrictive, and the filter cannot handle between-channel degradation.

A computational restoration filter for color images based on the idea of Hunt and Kübler is reported in Ohyama *et al.* [14]. It decorrelates the between-channel color components before applying independent restoration separately to each color component. Other reported color image restoration algorithms, for example Bescos *et al.* [2], apply conventional filtering to individual color components without using between-channel information.

There is much to be gained by incorporating in the restoration process both the between-channel and within-channel correlation of the multichannel image. Such a minimum mean-square error (MMSE) Wiener filter, which does not require the separability assumption as required in [8], has been developed for between-channel

Manuscript received December 15, 1989; revised September 25, 1990. This work was supported by the National Science Foundation under Grants ECS-8352356 and ATM-8414467, and in part by NASA under Grant NAG 5-580.

N. P. Galatsanos is with the Department of Electrical and Computer Engineering, Illinois Institute of Technology, Chicago, IL 60616.

R. T. Chin is with the Department of Electrical and Computer Engineering, University of Wisconsin, Madison, WI 53706.

IEEE Log Number 9101881.

restoration. Its results are reported by Galatsanos and Chin in [6]. However, the filter assumes that the image signal is spatially stationary and the degradation is shift invariant.

The stationarity assumption of the signal autocorrelation is recognized to be restrictive and unrealistic; the image data are assumed to have mean and variance independent of spatial location, while most real world images are nonstationary. This problem can be alleviated by the adaptive processing of signals via Kalman filtering.

The Kalman filter is an iterative MMSE procedure that adapts to local changes of the signal. The disadvantage of such a filter when applied to images is that it was derived for one-dimensional signals and its two-dimensional extension is still under investigation by many researchers.

There are two different approaches for two-dimensional Kalman filtering. In the first approach, a pixel-by-pixel scanning order is defined and the image is transformed into a one-dimensional signal. One widely known algorithm using this approach is the reduced update Kalman filter by Woods and Ingle [20]. It is based on a nonsymmetric half-plane (NSHP) model for the image signal and the updating process is limited to elements near the present data point for the purpose of reducing computation and storage. Recently, an extension of this filter was proposed by Tekalp and Pavlovic [18] for the restoration of color images. A NSHP multichannel color image model was estimated from prototype images and restoration experiments were reported in the RGB and YIQ domains.

The second approach is a line-by-line processing procedure. A number of researchers, including Biemond *et al.* [3], have explored this approach. It uses a semicausal image model which results in Toeplitz matrix structures in the image model and observation equations. Using the Toeplitz-to-circulant approximation, the line-by-line Kalman filter is then reduced to a parallel bank of low order Kalman filters realized in the Fourier domain.

In this paper the two-dimensional Kalman formulation of Biemond *et al.* [3] is used for multichannel restoration. Information distributed across image planes is utilized; thus all channels are processed simultaneously as a single entity. Using this approach, multichannel images are restored optimally because both the between-channel correlation and degradation are incorporated into the process. Both stationary and nonstationary image models for the multichannel filter have been developed. Section II presents the multichannel imaging model. Section III describes the multichannel degradation model. In Section IV the Kalman filter equations for multichannel images are derived and a fast algorithm is presented. Section V presents a nonstationary image model for the restoration filter. In Section VI color imagery, a special case of multichannel images, is considered and color restoration in the YIQ domain is explored. Section VII presents experiments that were performed to test the proposed multichannel Kalman filter. Finally, Section VIII contains our conclusions.

II. Multichannel Image Model

Let an image with N channels each of size $M \times M$ be modeled by a multichannel autoregressive model given by

$$f^o(i,j) = \sum_{n=1}^{N} \sum_{(p,q)\in R} a^{(o,n)}(p,q) \cdot f^n(i-p, j-q) + u^o(i,j) \quad \text{for } o = 1, 2, \cdots, N \text{ and } i, j = 1, 2, \cdots, M \tag{2.1a}$$

where f^o and u^o are the image and the noise process of the mth channel, respectively. The term $a^{(o,n)}$ represents the model coefficients, and R is the region of support. The sum over index n in (2.1) represents between-channel relations. Using a semicausal model, R is defined as

$$R = [(p,q) \mid 0 \le p \le p_2, \quad -q_1 \le q \le q_1] \tag{2.1b}$$

which is shown in Fig. 1.

$$E[u^o(i,j)^2] = E\left[\left\{f^o(i,j) - \sum_{n=1}^{N} \sum_{(z,w)\in R} a^{(o,n)}(z,w) \cdot f^n(i-z, j-w)\right\}^2\right] \tag{2.2}$$

is minimum. Minimizing (2.2) by setting

$$\frac{\partial\{E[u^o(i,j)^2]\}}{\partial\{a^{(o,b)}(l,k)\}} = E[u^o(i,j) f^h(i-l, j-k)] = 0 \quad \text{with } (l,k) \in R \tag{2.2a}$$

where $(l,k) \in R$, yields a set of multichannel normal equations

$$r_f^{(o,b)}(l,k) - \sum_{m=1}^{N} \sum_{(p,q)\in R} a^{(o,m)}(p,q) r_f^{(b,m)}(l-p, k-q) = \sigma^2_{(o,o)}\, \delta(l)\, \delta(k)\, \delta(o-b) \tag{2.3}$$

where

$$r_f^{(o,b)}(l,k) = E[f^o(i,j) f^b(i-l, j-k)] \tag{2.4a}$$

is the covariance of the signal f and

$$\sigma^2_{(o,o)} = E[\{u^o(i,j)\}^2] \tag{2.4b}$$

is the covariance of the driving noise and

$$\delta(i) = \begin{cases} 1 & i = 0 \\ 0 & \text{elsewhere.} \end{cases}$$

The coefficients $a^{(o,n)}$ can then be obtained by solving the normal equations (2.3).

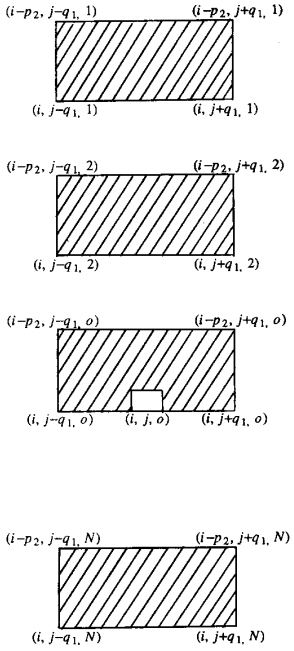

Fig. 1. The region of support at location (i, j, o) of the multichannel semicausal image model of (2.1a) and (2.1b). Indexes i, j specify the spatial location, and the index o the channel.

The autocovariance function of the driving noise is

$$r_u^{(o,h)}(l,k) = E[u^o(i,j)u^h(i-l,j-k)]$$
$$= E\Big[u^o(i,j)f^h(i-l,j-k) - \sum_{m=1}^{N}\sum_{(p,q)\in R} a^{(h,m)}(p,q)u^o(i,j) \cdot f^m(i-l-p,j-k-q)\Big]. \quad (2.5)$$

At $(l, k) = (0, 0)$, the second term of (2.5) is zero because of the orthogonality principle, and only the first term contributes to the covariance. At $l + p = 0$ and $k + q = 0$, the first term of (2.5) is zero and only the second term contributes to the covariance. Since (l, k) and $(p, q) \in R$, we have $0 \le (l, p) \le p_2$ and $-q_1 \le (k, q) \le q_1$ which yields $l = p = 0$. The noise covariance then becomes

$$r_u^{(o,h)}(l,k) = \begin{cases} \sigma^2_{(o,o)} & (l,k) = (0,0) \text{ and } h = o \\ \sigma^2_{(o,o)}[a^{(o,h)}(0,k)] & (0,k) \in R \\ 0 & \text{elsewhere.} \end{cases} \quad (2.6)$$

Unlike causal models, semicausal minimum variance models are not driven by white noise (see [9]). Thus the noise process $u^o(i, j)$ is correlated along the noncausal direction of our model (horizontal) and is also correlated between channels.

Equation (2.1) can be expanded as

$$f^o(i,j) = \sum_{(p,q)\in R} a^{(o,1)}(p,q)f^1(i-p,j-q) + \sum_{(p,q)\in R} a^{(o,2)}(p,q)f^2(i-p,j-q) + \cdots + \cdots + \sum_{(p,q)\in R} a^{(o,N)}(p,q) \cdot f^N(i-p,j-q) + u^o(i,j)$$
$$\text{for } o = 1, 2, \cdots, N \quad \text{and} \quad i, j = 2, \cdots, M. \quad (2.7)$$

Substituting the sums in the horizontal direction with matrix vector multiplications (2.7) yields

$$B_0^o \bar{u}^o(i) = \sum_{n=1}^{N}\sum_{p=0}^{p_2} [A^{(o,n)}(p)\bar{f}^n(i-p) + EL^{(o,n)}(p)\bar{f}^n_L(i-p) + ER^{(o,n)}(p)\bar{f}^n_R(i-p)] \quad (2.8)$$

with

$$\bar{f}^n(i) = [f^n(i,1), f^n(i,2), \cdots, f^n(i,M)]^t$$
$$\bar{u}^n(i) = [u^n(i,1), u^n(i,2), \cdots, u^n(i,M)]^t \quad (2.9)$$

$$a^{(o,n)}(0,0) = -1.0 \quad \text{for } o = n,$$

$$A^{(o,n)}(p) = \begin{bmatrix} -a^{(o,o)}(p,0) & \cdots & -a^{(o,n)}(p,-q_1) & \cdots & 0 & \cdots & 0 \\ \vdots & & \vdots & & -a^{(o,n)}(p,-q_1) & & \vdots \\ -a^{(o,n)}(p,q_1) & \cdots & -a^{(o,n)}(p,0) & & \vdots & & 0 \\ 0 & & \vdots & & -a^{(o,n)}(p,0) & \cdots & -a^{(o,n)}(p,-q_1) \\ \vdots & & -a^{(o,n)}(p,q_1) & & \vdots & & \vdots \\ \vdots & & \vdots & & \vdots & & \vdots \\ 0 & \cdots & 0 & \cdots & -a^{(o,n)}(p,q_1) & \cdots & -a^{(o,n)}(p,0) \end{bmatrix} \quad (2.10)$$

and B_0^o is an $M \times M$ identity matrix. Matrix $A^{(o,n)}$ is $M \times M$ Toeplitz, and matrices $EL^{(o,n)}$ and $ER^{(o,n)}$ are upper and lower triangular matrices, respectively, of dimension M

$\times q_1$. They represent the boundary coefficients. The $q_1 \times 1$ vectors $f_L(i-p)$ and $f_R(i-p)$ for $(i = 1, 2, \cdots, M)$ and $(p = 1, 2, \cdots, p_2)$ are the left and right boundaries. These, combined with the top boundary $f^n(i-p)$ for $(p = 1, 2, \cdots, p_2)$ and $(k = 1, 2, \cdots, N)$, are necessary to evaluate the image inside the $M \times M$ viewing area according to (2.8). These boundary conditions must be consistent with the statistical model of the image field and $\bar{f}_R^n$, $\bar{f}_L^n$, and $\bar{f}^n$ are set to be equal to the mean value of the image field. A more elaborate approach to the image boundary problem can be found in [21]. However, the improvement in visual quality at the image borders by using this elaborate approach is reportedly small [3]. Therefore, following [3] we set the boundary conditions equal to the mean value, in our case zero. Then (2.8) simplifies to

$$B_0^o \bar{u}^o(i) = \sum_{n=1}^{N} \sum_{p=0}^{p_2} A^{(o,n)}(p) \bar{f}^n(i-p) \qquad (2.11)$$

for

$$o = 1, 2, \cdots, N \quad \text{and} \quad i, j = 1, 2, \cdots, M.$$

For multichannel implementation of the Kalman filter, each iteration is applied to a single row across all channels simultaneously. For this purpose the multichannel image model in (2.11) must be written in a form which allows this type of processing. The summations over the channel index n and the image model vertical support index p are substituted by matrix-vector multiplications. Equation (2.11) then yields

$$\boldsymbol{s}(i) = \bar{\boldsymbol{A}}\boldsymbol{s}(i-1) + \bar{\boldsymbol{B}}\boldsymbol{u}(i) \qquad (2.12)$$

where

$$\bar{\boldsymbol{A}} = \begin{bmatrix} [\boldsymbol{A}^{-1}(0)\boldsymbol{A}(1)] & \cdots & [\boldsymbol{A}^{-1}(0)\boldsymbol{A}(p_2-1)] & [\boldsymbol{A}^{-1}(0)\boldsymbol{A}(p_2)] \\ \boldsymbol{I} & \cdots & \boldsymbol{0} & \boldsymbol{0} \\ \boldsymbol{0} & \cdots & \boldsymbol{0} & \boldsymbol{0} \\ \vdots & \cdots & \vdots & \vdots \\ \boldsymbol{0} & \cdots & \boldsymbol{I} & \boldsymbol{0} \end{bmatrix} \qquad (2.13)$$

is a matrix of dimension $p_2 \cdot NM \times p_2 \cdot MN$, $\boldsymbol{I}$ denotes an $NM \times MN$ identity matrix, $\boldsymbol{0}$ denotes a $NM \times MN$ zero matrix

$$\bar{\boldsymbol{B}} = \begin{bmatrix} [\boldsymbol{A}^{-1}(0)\boldsymbol{B}_0] \\ \boldsymbol{0} \\ \boldsymbol{0} \\ \vdots \\ \boldsymbol{0} \end{bmatrix} \qquad (2.14)$$

is a matrix of dimension $p_2 \cdot NM \times MN$, $\boldsymbol{B}_0$ a $NM \times MN$ identity matrix

$$\boldsymbol{s}(i) = [\boldsymbol{f}^t(i), \cdots, \boldsymbol{f}^t(i-p_2+1)]^t \qquad (2.15)$$

is a matrix of dimension $p_2 \times NM$

$$\boldsymbol{f}(i) = [\{\bar{f}^1(i)\}^t, \{\bar{f}^2(i)\}^t, \cdots, \{\bar{f}^N(i)\}^t]^t \qquad (2.16a)$$

$$\boldsymbol{u}(i) = [\{\bar{u}^1(i)\}^t, \{\bar{u}^2(i)\}^t, \cdots, \{\bar{u}^N(i)\}^t]^t \qquad (2.16b)$$

are multichannel vectors of dimension NM, and

$$\boldsymbol{A}(p) = \begin{bmatrix} [A^{(1,1)}(p)] & [A^{(1,2)}(p)] & \cdots & [A^{(1,N)}(p)] \\ [A^{(2,1)}(p)] & [A^{(2,2)}(p)] & \cdots & [A^{(2,N)}(p)] \\ \vdots & \vdots & \cdots & \vdots \\ [A^{(N,1)}(p)] & [A^{(N,2)}(p)] & \cdots & [A^{(N,N)}(p)] \end{bmatrix} \qquad (2.17)$$

is a $NM \times MN$ matrix. Equation (2.12) is the multichannel image model used in the Kalman equations.

III. Multichannel Degradation Model

A linear multichannel degradation with both within (spatial) and between-channel blur is assumed. The within-channel degradation is assumed to be shift invariant. However, a similar assumption for the between-channel degradation is not applicable. In many multichannel imaging systems, imaging characteristics vary from channel to channel: for example, in multispectral imaging, the wavelength at each channel is different. Assuming shift invariance for the between-channel blur, $(H^{(i,j)} = H^{(i+k,j+k)})$ forces all the within-channel degradations $H^{(i,i)}$ to be identical. This severely limits the applicability of the imaging model; for example, Bescos *et al.* [2] showed that for color images, chromatic aberrations result in different amounts of blur in each color plane.

Using the above assumptions the multichannel imaging equation is given by

$$g^m(i,j) = \sum_{n=1}^{N} \sum_{\lambda=-\lambda_1}^{\lambda_1} \sum_{k=-k_1}^{k_1} h^{m,n}(\lambda, k) \cdot f^n(i-\lambda, j-k) + v^m(i,j)$$
$$m = 1, 2, \cdots, N \quad \text{and} \quad i, j = 1, 2, \cdots, M \qquad (3.1)$$

where v^m is white additive noise and g^m is the observed image. Using the same philosophy as for the multichannel image model, (3.1) yields

$$\boldsymbol{g}(i) = \overline{\boldsymbol{H}}\boldsymbol{z}(i) = \boldsymbol{v}(i) \tag{3.2}$$

where $\boldsymbol{g}(i)$ and $\boldsymbol{v}(i)$ are vectors of length MN defined in the same way as $\boldsymbol{f}(i)$ in (2.16a)

$$z(i) = [\boldsymbol{f}^t(i + \lambda_1), \cdots, \boldsymbol{f}^t(i), \cdots, \boldsymbol{f}^t(i - \lambda_1)]^t \tag{3.3}$$

is a vector of length ΛMN, with $\Lambda = 2\lambda_1 + 1$

$$\overline{\boldsymbol{H}} = [\boldsymbol{H}(-\lambda_1), \cdots, \boldsymbol{H}(0), \cdots, \boldsymbol{H}(\lambda_1)] \tag{3.4}$$

is a matrix of dimension $MN \times MN\Lambda$

$$\boldsymbol{H}(\lambda) = \begin{bmatrix} [H^{(1,1)}(\lambda)] & [H^{(1,2)}(\lambda)] & \cdots & [H^{(1,N)}(\lambda)] \\ [H^{(2,1)}(\lambda)] & [H^{(2,2)}(\lambda)] & \cdots & [H^{(2,N)}(\lambda)] \\ \vdots & \vdots & \cdots & \vdots \\ [H^{(N,1)}(\lambda)] & [H^{(N,2)}(\lambda)] & \cdots & [H^{(N,N)}(\lambda)] \end{bmatrix} \tag{3.5}$$

is a $MN \times MN$ matrix, and

$$H^{(m,n)}(\lambda) = \begin{bmatrix} -h^{m,n}(\lambda, 0) & \cdots & -h^{m,n}(\lambda, -k_1) & \cdots & 0 & \cdots & 0 \\ \vdots & & \vdots & & -h^{m,n}(\lambda, -k_1) & & \vdots \\ -h^{m,n}(\lambda, k_1) & \cdots & -h^{m,n}(\lambda, 0) & & \vdots & & 0 \\ 0 & & \vdots & & \vdots & \cdots & -h^{m,n}(\lambda, -k_1) \\ \vdots & & -h^{m,n}(\lambda, k_1) & & -h^{m,n}(\lambda, 0) & & \vdots \\ \vdots & & \vdots & & \vdots & & \vdots \\ 0 & \cdots & 0 & \cdots & -h^{m,n}(\lambda, k_1) & \cdots & -h^{m,n}(\lambda, 0) \end{bmatrix} \tag{3.6}$$

is a $M \times M$ Toeplitz matrix.

If $p_2 + 1 \leq \Lambda = 2\lambda_1 + 1$, we can substitute $z(i)$ in the image model equation. Then (2.12) yields

$$z(i) = \tilde{\boldsymbol{A}}z(i - 1) + \tilde{\boldsymbol{B}}\boldsymbol{u}(i) \tag{3.7}$$

with

$$\tilde{\boldsymbol{A}} = \begin{bmatrix} [\boldsymbol{A}^{-1}(0)\boldsymbol{A}(1)] & [\boldsymbol{A}^{-1}(0)\boldsymbol{A}(2)] & \cdots & [\boldsymbol{A}^{-1}(0)\boldsymbol{A}(p_2)] & \boldsymbol{0} \cdots \boldsymbol{0} & \boldsymbol{0} \\ \boldsymbol{I} & \boldsymbol{0} & & \boldsymbol{0} & \boldsymbol{0} \cdots \boldsymbol{0} & \boldsymbol{0} \\ \boldsymbol{0} & \boldsymbol{I} & & \boldsymbol{0} & \boldsymbol{0} \cdots \boldsymbol{0} & \boldsymbol{0} \\ \vdots & \vdots & & \vdots & \vdots \cdots \vdots & \vdots \\ & & & & \boldsymbol{0} \cdots \boldsymbol{0} & \boldsymbol{0} \\ \boldsymbol{0} & \boldsymbol{0} & & \boldsymbol{0} & \boldsymbol{0} \cdots \boldsymbol{0} & \boldsymbol{0} \\ \boldsymbol{0} & \boldsymbol{0} & & \boldsymbol{I} & \boldsymbol{I} \cdots \boldsymbol{0} & \boldsymbol{0} \\ \vdots & \vdots & & \vdots & \vdots \cdots \vdots & \vdots \\ \boldsymbol{0} & \boldsymbol{0} & \cdots & \boldsymbol{0} & \boldsymbol{0} \cdots \boldsymbol{I} & \boldsymbol{0} \end{bmatrix} \tag{3.8}$$

and

$$\tilde{\boldsymbol{B}} = \begin{bmatrix} [\boldsymbol{A}^{-1}(0)\boldsymbol{B}_0] \\ \boldsymbol{0} \\ \boldsymbol{0} \\ \vdots \\ \boldsymbol{0} \\ \boldsymbol{0} \\ \vdots \\ \boldsymbol{0} \end{bmatrix}. \tag{3.9}$$

Matrix $\tilde{\boldsymbol{A}}$ is of dimension $\Lambda MN \times MN\Lambda$, matrix $\tilde{\boldsymbol{B}}$ is of dimension $\Lambda MN \times MN$, $\boldsymbol{I}$ is a $NM \times MN$ identity matrix, and $\boldsymbol{0}$ is a $NM \times MN$ a zero matrix. Equations (3.7) and (3.2) are the state and observation equations of the multichannel Kalman filter.

IV. Kalman Filter Equations

Following Sage and Melsa [15] and using (3.5) and (3.6) as the signal and observation equations, respectively, the Kalman filter equations for multichannel image

restoration are given as

$$\hat{z}(i) = \tilde{A}\hat{z}(i-1) + F(i)[g(i) - \overline{H}\tilde{A}\hat{z}(i-1)] \quad (4.1)$$

where the first and the second term of the right-hand side of (4.1) are the prediction and the correction term of the new estimate $\hat{z}(i)$, respectively. Matrix $F(i)$ is the Kalman gain which is given by

$$F(i) = Q(i-1)\overline{H}^t[\overline{H}Q(i-1)\overline{H}^t + \boldsymbol{R}_v(i)]^{-1}. \quad (4.2)$$

Matrix $Q(i)$ is the covariance of the error $[z(i) - \hat{z}(i)]$ and is given by

$$Q(i) = \tilde{A}[I - F(i)\overline{H}]Q(i-1)\tilde{A}^t + \tilde{B}\boldsymbol{R}_u(i)\tilde{B}^t \quad (4.3)$$

where $\boldsymbol{R}_v(i)$ is the covariance matrix of the observation noise vector $\mathbf{v}(i)$. For white noise that is uncorrelated between channels

$$\boldsymbol{R}_v(i) = \begin{bmatrix} \sigma_{11}^2 & \mathbf{0} & \cdots & \mathbf{0} \\ \mathbf{0} & \sigma_{22}^2\boldsymbol{I} & \cdots & \mathbf{0} \\ \vdots & \vdots & \cdots & \vdots \\ \mathbf{0} & \mathbf{0} & \cdots & \sigma_{NN}^2\boldsymbol{I} \end{bmatrix} \quad (4.4)$$

with

$$\sigma_{mm}^2 = E[v^m(i,j)^2].$$

The matrix $\boldsymbol{R}_u(i)$ is the covariance of the nonwhite image model driving noise $\boldsymbol{u}(i)$ and is defined by

$$\boldsymbol{R}_u(i) = E[\boldsymbol{u}(i)\boldsymbol{u}^t(i)]$$

$$= \begin{bmatrix} E[\bar{u}^1(\bar{u}^1)^t] & E[\bar{u}^1(\bar{u}^2)^t] & \cdots & E[\bar{u}^1(\bar{u}^N)^t] \\ E[\bar{u}^2(\bar{u}^1)^t] & E[\bar{u}^2(\bar{u}^2)^t] & \cdots & E[\bar{u}^2(\bar{u}^N)^t] \\ \vdots & \vdots & \cdots & \vdots \\ E[\bar{u}^N(\bar{u}^1)^t] & E[\bar{u}^N(\bar{u}^2)^t] & \cdots & E[\bar{u}^N(\bar{u}^N)^t] \end{bmatrix}. \quad (4.5)$$

From (2.6) we have

$$E[\bar{u}^m(i)\{\bar{u}^n(i)\}^i] = \sigma_{(m,m)}^2 A(0)^{(m,n)}\delta(i) \quad (4.6)$$

where $\sigma_{(m,n)}^2$ is defined in (2.4), and (4.5) can be written as

$$\boldsymbol{R}_u(i) = \delta(i) \times \begin{bmatrix} \sigma_{(1,1)}^2 A^{(1,1)}(0) & \sigma_{(1,1)}^2 A^{(1,2)}(0) & \cdots & \sigma_{(1,1)}^2 A^{(1,N)}(0) \\ \sigma_{(2,2)}^2 A^{(2,1)}(0) & \sigma_{(2,2)}^2 A^{(2,2)}(0) & \cdots & \sigma_{(2,2)}^2 A^{(2,N)}(0) \\ \vdots & \vdots & \cdots & \vdots \\ \sigma_{(N,1)}^2 A^{(N,1)}(0) & \sigma_{(N,N)}^2 A^{(N,2)}(0) & \cdots & \sigma_{(N,N)}^2 A^{(N,N)}(0) \end{bmatrix}. \quad (4.7)$$

Matrices $F(i)$, $Q(i)$, $\boldsymbol{R}_v(i)$, and $\boldsymbol{R}_u(i)$ in (4.1), (4.2), and (4.3) are of dimensions $\Lambda MN \times MN$, $\Lambda MN \times MN\Lambda$ $MN \times MN$, and $MN \times MN$, respectively. Computing $\hat{z}(i)$ from (4.1),-(4.3) directly is computationally expensive. It requires $O(M)$ multiplications of $\Lambda NM \times MN\Lambda$ matrices and M inversions of $MN \times MN$ matrices. For a modest example, a $128 \times 128 \times 3$ image with $\lambda_1 = k_1 = 2$, requires $O(128)$ multiplications of 1920×1920 matrices and 128 inversions of 384×384 matrices.

In monochrome image restoration, the Toeplitz-to-circulant approximation and the discrete Fourier transform (DFT) are commonly used to decouple the Kalman filter equations for fast computation (see Biemond *et al.* [3]). In order to alleviate the computational and storage requirement for the implementation of the multichannel Kalman restoration filter, the structure of the matrices involved in the computation is examined.

The matrices $\boldsymbol{A}(p)$ and $\boldsymbol{H}(\lambda)$ defined in (2.18) and (3.3) appear as submatrices in $\tilde{A}$ and $\overline{H}$ of the filter given by (4.1)-(4.3). Both $\boldsymbol{A}(p)$ and $\boldsymbol{H}(\lambda)$ contain submatrices $H^{(i,j)}(\lambda)$ and $A^{(i,j)}(p)$ which are $M \times M$ Toeplitz. However, $\boldsymbol{A}(p)$ itself is not Toeplitz, that is,

$$A^{(m,n)}(p) \neq A^{(m+k,n+k)}(p) \quad (4.8)$$

where $A^{(m,n)}$ and $A^{(m+k,n+k)}$ contains model coefficients of channels (m, n) and $(m + k, n + k)$, respectively. In general, different channels contain different characteristics of the scene being imaged; therefore, there is no justification for assuming that coefficients of different channels are equal. Similarly, $\boldsymbol{H}(\lambda)$ is not Toeplitz, that is,

$$H^{(m,n)}(\lambda) \neq H^{(m+k,n+k)}(\lambda) \quad (4.9)$$

because of the between-channel shift-variant blur assumption.

For the above reasons, the standard Toeplitz-to-circulant approximation as used in monochrome image restoration cannot be applied directly to multichannel restoration. The approximation can only be used for submatrices $A^{(i,j)}(p)$ and $H^{(i,j)}(\lambda)$ with $(i, j = 1, 2, \cdots, N)$, $(p = 0, \cdots, p_2)$ and $(\lambda = -\lambda_1, \cdots, 0, \cdots, \lambda_1)$ (see Andrews and Hunt [1]). After the circulant approximation, the matrices in (4.1)-(4.3) become block matrices of the following form:

$$\begin{bmatrix} C^{11} & C^{12} & \cdots & C^{1Q} \\ C^{21} & C^{22} & \cdots & C^{2Q} \\ \vdots & \vdots & \cdots & \vdots \\ C^{P1} & C^{P2} & \cdots & C^{PQ} \end{bmatrix} \quad \text{(Form C)}$$

where the entire matrix is not circulant but its submatrices C^{ij} are circulant. The above matrix structure is denoted as the form-C matrix. Form-C matrices can be transformed to matrices of the following form:

$$\begin{bmatrix} [D^{11}] & [D^{12}] & \cdots & [D^{1Q}] \\ [D^{21}] & [D^{22}] & \cdots & [D^{2Q}] \\ \vdots & \vdots & \cdots & \vdots \\ [D^{P1}] & [D^{P2}] & \cdots & [D^{PQ}] \end{bmatrix} \quad \text{(Form D)}$$

via the DFT [5], where $[D^{ij}]$ are $M \times M$ diagonal matrices.

After the Toeplitz-to-circulant approximation the Form-C matrices $\tilde{A}^c$, $F(i)^c$, $Q(i)^c$, $R(i)_u^c$, and $R(i)_v^c$ in (4.1)–(4.3) can be transformed to form-D matrices, giving

$$\hat{Z}(i) = \tilde{A}^D \hat{Z}(i-1) + F^D(i)[G(i) - \overline{H}^D \tilde{A}^D \hat{Z}(i-1)] \tag{4.10}$$

$$F^D(i) = Q^D(i-1)(\overline{H}^D)^t \cdot [\overline{H}^D Q^D(i-1)(\overline{H}^D)^t + R_v^D(i)]^{-1} \tag{4.11}$$

$$Q^D(i) = \tilde{A}^D[I - F^D(i)\overline{H}^D]Q^D(i-1) \cdot (\tilde{A}^D)^t + \tilde{B}^D R_u^D(i)(\tilde{B}^D)^t \tag{4.12}$$

where $\hat{Z}(i)$ and $G(i)$ are the DFT of $\hat{z}(i)$ and $g(i)$, respectively. The superscript D in the above equations indicates form-D matrices. Since form-D matrices are closed under multiplication addition and inversion, the computations in (4.10)–(4.12) can be performed efficiently [6].

Based on the above, the multichannel Kalman filter is implemented by the following steps:

Step 1: Diagonalize $A^{(m,n)}(p)$ and $H^{(m,n)}(\lambda)$ using the DFT for $m, n = 1, 2, \cdots, N$, $-\lambda_1 \le \lambda \le \lambda_1$, and $0 \le p \le p_2$ where λ_1 and p_2 define the region of support of the degradation and the image mode, respectively.

Step 2: Transform $\bar{g}^m(i)$ using $\overline{G}^m(i) = W^{-1}\bar{g}^m(i)$ for $i = 1, 2, \cdots, M$ and $m = 1, 2, \cdots, N$ and construct $G(i)$.

Step 3: Construct matrices $\tilde{A}^D$, $\tilde{B}^D$, and $\overline{H}^D$.

Step 4: For $i = 1, 2, \cdots, N$ compute (4.13)–(4.15) to solve for $\hat{Z}(i)$, the Kalman solution. Use the iterative procedure of Lemma 2 in [6] for the matrix inversion in (4.11).

Step 5: Inverse DFT of $\hat{Z}(i)$.

From the definition of $z(i)$ in (3.7) it is easy to see that $\hat{f}(i)$ is contained in all $\hat{z}(j)$ with $j = i - \lambda_1, \cdots, i, \cdots, i + \lambda_1$. In our implementation $\hat{f}(i)$ is obtained from the λ_1 − lag estimate of $z(i)$ by

$$\hat{f}(i) = [\mathbf{0}, \mathbf{0}, \cdots, I]\hat{z}(i + \lambda_1).$$

In this case $\hat{f}(i)$ is updated $\Lambda = 2\lambda_1 + 1$ times, yielding the smallest estimation error. Using the above method, the multichannel restoration problem can be solved even when NM is large.

V. Nonstationary Image Model

The Kalman filter implementation of (4.1)–(4.3) has been derived from the imaging model of (2.17). This imaging model is a fixed model for the entire image. It lacks the flexibility to take into account the local changes of image statistics. An improved model that adapts to spatial variations is given by

$$\sum_{p=0}^{p_2} A^{(i)}(p) f(i-p) = B_0^{(i)} u(i). \tag{5.1}$$

Using (5.1) the Kalman equations (4.1)–(4.3) become

$$\hat{z}(i) = [\tilde{A}^{(i)}]\hat{z}(i-1) + F(i)[g(i) - \overline{H}[\tilde{A}^{(i)}]\hat{z}(i-1)] \tag{5.2}$$

$$F(i) = Q(i-1)[\overline{H}]^t[\overline{H}Q(i-1)[\overline{H}]^t + R_v(i)]^{-1} \tag{5.3}$$

$$Q(i) = [\tilde{A}^{(i)}][I - F(i)\overline{H}]Q(i-1)[\tilde{A}^{(i)}]^t + [\tilde{B}^{(i)}]\overline{R}_u(i)[\tilde{B}^{(i)}]^t \tag{5.4}$$

where $R_v(i)$ is the covariance matrix of the noise vector $v(i)$ and is defined in the same way as the stationary model in (4.4). The matrix $\overline{R}_u(i)$ is the spatially varying covariance of $u(i)$. For the nonstationary model, $\overline{R}_u(i)$ has the same definition as in (4.5) and (4.7); however, (4.6) becomes

$$E[\bar{u}^m(i)\{\bar{u}^n(i)\}^t] = [\sigma_{(m,n)}^{(i)}]^2[A^{(i)}(0)^{(m,n)}]\delta(i) \tag{5.5}$$

where

$$[\sigma_{(m,n)}^{(i)}]^2 = E[u^m(i,j)u^n(i,j)]. \tag{5.6}$$

The index i in (5.5) and (5.6) indicates the spatially varying nature of the image model. Note that a spatially varying degradation $\overline{H}^{(i)}$ can be included in the nonstationary model without any additional complications. This nonstationary Kalman filter is implemented in a similar way as the stationary filter. Equations (5.2)–(5.4) are solved using the 5-step process previously described.

VI. Restoration of Color Images in the YIQ Domain

Color imagery is a special case of multichannel images. For most color images the three RGB color planes exhibit strong between-channel correlations. In order to decorrelate the three color planes the RGB-to-YIQ transformation has been used and reported in [15]. This transformation can be viewed as a between-color Karhunen–Loeve transformation (see [16] and [8]). The RGB-to-YIQ transformation is defined by

$$\begin{bmatrix} f_Y(i,j) \\ f_I(i,j) \\ f_Q(i,j) \end{bmatrix} = \begin{bmatrix} 0.299 & 0.587 & 0.114 \\ 0.596 & -0.274 & -0.322 \\ 0.211 & -0.523 & 0.312 \end{bmatrix} \begin{bmatrix} f_R(i,j) \\ f_G(i,j) \\ f_B(i,j) \end{bmatrix}. \tag{6.1}$$

In the YIQ domain, the multichannel imaging equation (3.1) for $M \times M$ color images can be written as

$$\tilde{g} = \tilde{H}T^{-1}T\tilde{f} + \tilde{v} \tag{6.2}$$

where $\tilde{g}$, $\tilde{f}$, and $\tilde{v}$ are $3M^2$ vectors, representing the observed, original, and noise signal, respectively. The $3M^2 \times 3M^2$ matrix $\tilde{H}$ represents the color degradation [4]. The linear RGB-to-YIQ transformation T is defined by

$$T = \begin{bmatrix} 0.299I & 0.587I & 0.114I \\ 0.596I & -0.274I & -0.322I \\ 0.211I & -0.523I & 0.312I \end{bmatrix} \tag{6.3}$$

where I is an $M^2 \times M^2$ identity matrix. Using (6.2) as the imaging equation the stored color image can be computed in the YIQ domain from image data given in the RGB domain.

The transformed degradation is given by

$$\tilde{H}T^{-1} = \tilde{H}\begin{bmatrix} 1.0I & 0.956I & 0.621I \\ 1.0I & -0.272I & -0.647I \\ 1.0I & -1.106I & 1.703I \end{bmatrix} \tag{6.4}$$

where the coefficients of T^{-1} are computed as

$$\begin{bmatrix} 0.299 & 0.587 & 0.114 \\ 0.596 & -0.274 & -0.322 \\ 0.211 & -0.523 & 0.312 \end{bmatrix}^{-1} = \begin{bmatrix} 1.0 & 0.956 & 0.621 \\ 1.0 & -0.272 & -0.647 \\ 1.0 & -1.106 & 1.703 \end{bmatrix}.$$

The transformed degradation contains between-channel degradation components even when the original $\tilde{H}$ contains only spatial blur. Thus, restoration in the YIQ domain cannot simplify to independent channel restoration even when there is no between-channel blur in the original RGB image data. A similar approach was used in [18] for restoration of color images in the YIQ domain. It was assumed that the observed data are in the YIQ domain as defined by the following imaging equation:

$$T\tilde{g} = T\tilde{H}T^{-1}T\tilde{f} + T\tilde{v}. \tag{6.5}$$

Using this approach, the observation noise is also transformed in the YIQ domain, yielding correlated between-channel noise. In the special case considered in [18], all channels were only spatially degraded by the same blur, thus the degradation $T\tilde{H}T^{-1}$ had no between-channel component. However, in the general case using the approach in [18], both the noise covariance and the degradation will contain between-channel components.

VII. Experiments

Experiments were performed to test the multichannel Kalman filter. In many imaging systems, where the physical process that generates the observed images is known, it is not unreasonable to assume that the degradation can be correctly estimated. In addition, the problem of blind estimation of image noise variance has had some success (see [1] and [13]). Thus in our experiments we assumed that both the degradation and the noise variance were known.

The Toeplitz-to-circulant approximation was computed using the DFT, whereby the Toeplitz matrix was first transformed by a similarity transformation and then the off-diagonal elements were set to zero. Image models with $p_2 = q_2 = 1$ were used in all the experiments. As a measure of filter performance, we used both the MSE and the percentage of improvement defined by

$$I\% = 100 \times \left[1 - \frac{\|\hat{f} - f\|^2}{\|g - f\|^2}\right]\% \tag{7.1}$$

where $\|\cdot\|$ is the L_2 norm, f is the ideal image, $\hat{f}$ is the restored image plane, and g is the observed image plane.

Experiment One: This experiment was designed to test multichannel Kalman filtering when identical channels are spatially degraded. This situation may arise when motion compensated multiple time frames are being restored, or when the same scene is imaged by different sensors (see [7] and [10]). A multichannel test image constructed by a set of identical images was used.

The green color plane of the Lena 128×128 image was chosen to construct a three-channel image. Known spatial degradation $\tilde{H}$ was applied, where $\tilde{H}$ is given by

$$\tilde{H} = \begin{bmatrix} H^{(R,R)} & 0 & 0 \\ 0 & H^{(G,G)} & 0 \\ 0 & 0 & H^{(B,B)} \end{bmatrix} \tag{7.2}$$

and $H^{(i,j)}$ are $M^2 \times M^2$ block Toeplitz submatrices representing linear-motion blurring filters implemented as convolution masks. Submatrix $H^{(R,R)}$ represents a 1×5 uniform convolution operator with $1/5$ weights in the R channel; $H^{(G,G)}$ a 1×7 mask with $1/7$ weights in G; and $H^{(B,B)}$ a 1×9 mask with $1/9$ weights in B. Finally, independent white Gaussian noise was added to each degraded image plane, resulting in 20, 30, and 40 dB SNR in channels R, G, and B, respectively. The SNR was defined by

$$\text{SNR} = 10 \log \frac{\|f_i\|^2}{\|n_i\|^2}. \tag{7.3}$$

Single and multichannel Kalman filtering was used in the restoration. The image model was estimated from the degraded image. Since the multichannel image consists of different degraded versions of the same signal, the multichannel model contains more information and thus yields better restoration. The MSE results of this experiment are tabulated in Table I.

TABLE I
EXPERIMENT ONE: KALMAN FILTER RESTORATION OF THE THREE IDENTICAL GREEN PLANES OF THE LENA 128 × 128 IMAGE. THE SNR WAS 20, 30, AND 40 dB FOR CHANNELS 1, 2, AND 3, RESPECTIVELY. 1 × 5, 1 × 7, AND 1 × 9 BLURS WERE USED FOR THE RESPECTIVE CHANNELS. THE IMAGE MODELS WERE COMPUTED FROM THE DEGRADED IMAGE $\boldsymbol{g}$

Mean-Square Error (Percentage Improvement%)			
	Channel 1	Channel 2	Channel 3
Without restoration	9.54 (0%)	11.23 (0%)	12.88 (0%)
Independent restoration	7.92 (16%)	7.88 (30%)	6.64 (48%)
Multichannel restoration	6.86 (28%)	5.46 (51%)	5.34 (59%)

Experiment Two: This experiment was designed to test the multichannel Kalman filter in restoring images with correlated channels degraded only by spatial blur. Color imagery was used as an example. Restoration of color images was performed both in the RGB and in the YIQ domain, and image models were estimated from both the original $\boldsymbol{f}$ and the degraded $\boldsymbol{g}$ image. Finally, both stationary and nonstationary image models were tested.

The RGB components of the 128 × 128 Lena color image were blurred with the same degradation $\tilde{\boldsymbol{H}}$ as in experiment one. Two sets of observed images were generated by adding white Gaussian noise to the blurred images. In the first set the SNR was 10, 20, and 30 dB and in the second, 20, 30, and 40 dB for channels R, G, and B, respectively.

The original and degraded images were used to estimate both the single and multichannel image models in the RGB domain. As expected, in both cases multichannel filtering gave better results, both visually and by MSE. This was expected since the three channels are highly correlated in the RGB domain, thus the multichannel image model contains cross-channel coefficients used in restoration whereas the single-channel model treats each channel separately.

Restoration in the YIQ domain was tested. The original images were used to estimate the image models. Multichannel restoration was used with the transformed degradation matrix $\tilde{\boldsymbol{H}}\boldsymbol{T}^{-1}$. Single-channel restoration is not applicable in this case (see Section VI). The multichannel Kalman filter was tested using both multichannel (with between-channel coefficients) and single-channel (without between-channel coefficients) image models. The single-channel image model produced better results. This was expected, since transformation to the YIQ domain decorrelates between-channel components, resulting in independent signals across channels. In order to quantify the between-channel decorrelation property of the RGB-YIQ transform, a between-channel correlation measure S_{ij} was used and is given by

$$S_{ij} = \left(\frac{f_i}{\| f_i \|}, \frac{f_j}{\| f_j \|} \right) \tag{7.4}$$

where $(,)$ is the inner product, $\| \ \|$ the L_2 norm, and i, j the channel indices. The S_{ij} for the test image were computed in the RGB and in the YIQ domain and are tabulated in Tables II and III. From these tables we can see the between-channel correlations are significantly smaller in the YIQ domain than in the RGB domain.

TABLE II
VALUES OF THE SIMILARITY MEASURE S_{ij} GIVEN BY (7.3) FOR THE R, G, AND B COLOR PLANES OF THE LENA 128 × 128 IMAGE

$S_{RR} = 1.0$	$S_{RG} = 0.88$	$S_{RB} = 0.68$
$S_{GR} = 0.88$	$S_{GG} = 1.0$	$S_{RB} = 0.91$
$S_{BR} = 0.68$	$S_{BG} = 0.91$	$S_{BB} = 1.0$

TABLE III
THE VALUES OF THE SIMILARITY MEASURE S_{ij} GIVEN BY (7.3) FOR THE Y, I, AND Q PLANES OF THE LENA 128 × 128 IMAGE

$S_{YY} = 1.0$	$S_{YI} = -0.22$	$S_{YQ} = -0.76$
$S_{IY} = -0.22$	$S_{II} = 1.0$	$S_{IQ} = 0.31$
$S_{QY} = -0.76$	$S_{QI} = 0.31$	$S_{QQ} = 1.0$

The nonstationary image model described in Section V was also tested in this experiment. The model coefficients were estimated from the original image $\boldsymbol{f}$ with $p_2 = q_2 = 1$. To estimate the ith model, rows $(i - L)$ to $(i + L)$ from the original image data were used. It was observed experimentally that $L = 16$ produces the best results for the color Lena image.

The results of this experiment are tabulated in Tables IV and V. Images used in this experiment corresponding to Table V are shown in Fig. 2. from Tables IV and V we observe that multichannel restoration in the RGB domain yields better MSE results than multichannel restoration in the YIQ domain. This is expected, since the YIQ transformation is a fixed transformation independent of the input image signal, approximating the between-color Karhunen–Loeve transform. From Table III and IV we also observe that the nonstationary image model yields better results than the stationary model. However, the MSE improvement is small and virtually undetected visually.

Experiment Three: This experiment was designed to test the multichannel Kalman filter in the presence of between-channel blur. This type of degradation is encountered in remote sensing of multispectral satellite images. Less than ideal spectral characteristics of detectors produce leakage between adjacent spectral bands, resulting in between-channel degradation.

The same Lena color image was used. The known degradation matrix $\tilde{\boldsymbol{H}}$ is given by

$$\tilde{\boldsymbol{H}} = \begin{bmatrix} 0.50H^{(R,R)} & 0.25H^{(R,G)} & 0.25H^{(R,B)} \\ 0.25H^{(G,R)} & 0.50H^{(G,G)} & 0.25H^{(G,B)} \\ 0.25H^{(B,R)} & 0.25H^{(B,G)} & 0.50H^{(B,B)} \end{bmatrix} \tag{7.5}$$

where $H^{(i,j)}$ are $M^2 \times M^2$ block Toeplitz submatrices representing low-pass blurring filters implemented as convolution masks. The submatrices $H^{(R,R)}$, $H^{(R,G)}$, and $H^{(R,B)}$ were implemented as 1 × 5 convolution operators with 1/5 weights; $H^{(G,R)}$, $H^{(G,G)}$, and $H^{(G,B)}$ were 5 × 5 masks with 1/25 weights; $H^{(B,R)}$, $H^{(B,G)}$, and $H^{(B,B)}$ were

TABLE IV
EXPERIMENT TWO: MULTICHANNEL KALMAN RESTORATION OF THE COLOR LENA 128 × 128 IMAGE. UNIFORM 1 × 5, 1 × 7, AND 1 × 9 BLURS WERE USED FOR CHANNELS R, G, AND B, RESPECTIVELY. THE SNR WAS 10, 20, 30 dB IN CHANNELS R, G, AND B, RESPECTIVELY

Mean-Square Error (Percentage Improvement%)	Channel R	Channel G	Channel B
Without restoration	8.47 (0%)	11.51 (0%)	8.59 (0%)
(i) Independent-channel restoration, using f to estimate the image model.	6.30 (26%)	7.95 (31%)	3.99 (53%)
(ii) Multichannel restoration, using f to estimate the image model.	4.92 (42%)	5.46 (53%)	3.39 (60%)
(iii) Independent-channel restoration, using g to estimate the image model.	6.70 (21%)	9.32 (19%)	6.14 (28%)
(iv) Multichannel restoration, using g to estimate the image model.	5.98 (29%)	7.52 (35%)	5.57 (35%)
(v) Restoration in the YIQ domain without between-channel coefficients in the image model.	4.89 (42%)	6.25 (46%)	3.63 (58%)
(vi) Restoration in the YIQ domain with between-channel coefficients in the image model.	7.59 (10%)	6.67 (42%)	4.79 (44%)
(vii) Multichannel restoration using a nonstationary model estimated from f.	4.56 (46%)	5.03 (56%)	3.08 (64%)

The results of the experiments are: (i) Independent-channel restoration, using the original image f to estimate the image model. (ii) Multichannel restoration, using the original image f to estimate the image model. (iii) Independent-channel restoration, using the degraded image g to estimate the image model. (iv) Multichannel restoration, using the degraded image g to estimate the image model. (v) Restoration in the YIQ domain without between-channel coefficients in the image model. (vi) Restoration in the YIQ domain with between-channel coefficients in the image model. (vii) Multichannel restoration using a nonstationary model estimated from the original image f.

TABLE V
EXPERIMENT TWO: MULTICHANNEL KALMAN RESTORATION OF THE COLOR LENA 128 × 128 IMAGE. UNIFORM 1 × 5, 1 × 7, AND 1 × 9 BLURS WERE USED FOR CHANNELS R, G, AND B, RESPECTIVELY. THE SNR WAS 20, 30, 40 dB IN CHANNELS R, G, AND B, RESPECTIVELY

Mean-Square Error (Percentage Improvement)	Channel R	Channel G	Channel B
Without restoration	6.30 (0%)	11.23 (0%)	8.57 (0%)
(i) Independent-channel restoration, using f to estimate the image model.	4.60 (27%)	5.44 (52%)	2.32 (73%)
(ii) Multichannel restoration using f to estimate the image model.	2.90 (54%)	2.95 (74%)	1.76 (80%)
(iii) Independent-channel restoration, using g to estimate the image model.	5.24 (17%)	7.88 (30%)	4.51 (48%)
(iv) Multichannel restoration, using g to estimate the image model.	3.58 (43%)	5.38 (52%)	4.09 (52%)
(v) Restoration in the YIQ domain without between-channel coefficients in the image model.	3.07 (51%)	3.93 (65%)	1.98 (77%)
(vi) Restoration in the YIQ domain with between-channel coefficients in the image model.	6.36 (−1%)	4.16 (64%)	3.42 (60%)
(vii) Multichannel restoration using a nonstationary model estimated from f.	2.68 (58%)	2.72 (76%)	1.60 (81%)

The results of the experiments are: (i) Independent-channel restoration, using the original image f to estimate the image model. (ii) Multichannel restoration, using the original image f to estimate the image model. (iii) Independent-channel restoration, using the degraded image g to estimate the image model. (iv) Multichannel restoration, using the degraded image g to estimate the image model. (v) Restoration in the YIQ domain without between-channel coefficients in the image model. (vi) Restoration in the YIQ domain with between-channel coefficients in the image model. (vii) Multichannel restoration using a nonstationary model estimated from the original image f.

5 × 1 masks with 1/5 weights. Finally, independent-white Gaussian noise was added to each degraded image plane, generating two sets of images. The first set had SNR = 20 dB in each channel, and the second, 30 dB.

For comparison purposes the degraded color image was first restored by the single-channel Kalman filter of the Biemond *et al.* [3]. It was applied independently to each of the three color channels, using only spatial degradation. Next, the multichannel Kalman filter was applied using between-channel degradation, and only within-channel model coefficients of (2.1) were used. Finally, the multichannel Kalman filter was applied using both between-channel degradation and between-channel image model coefficients.

The MSE results of this experiment are tabulated in Tables VI and VII. Images of this experiment corresponding to Table VII are shown in Fig. 3. As expected, neglecting between-channel degradation produces poor results. Ringing artifacts are observed in Fig. 3(b) in channels B and G of the independent-channel restoration. The line-by-line approach of this Kalman filter implementation requires a boundary condition for blurs that have a vertical component. Since circulant convolution was used to degrade the channels vertically the degraded image in a circulant order was used as the boundary condition. However, independent-channel restoration neglects between-channel degradation; thus there is a discrepancy between the boundary condition and the degradation model. This discrepancy resulted in the ringing artifacts in Fig. 3(b). Experiments using zero boundary conditions were conducted. Similar results were observed, however, the ringing was more severe because the discrepancy of this boundary condition is worse. When the between-channel degradation was used, the ringing artifacts disappeared and the average intensity of the restored images was nearly equal to the original average (see channel G in Fig. 3(b) and (c). Further improvements was observed when the between-channel model coefficients were used in the restoration process.

Experiment Four: This experiment repeated experiment three using a different color test image. The color

(a)

(b)

(c)

Fig. 2. (a) The original color Lena image. The left image is the red channel, the middle is the green channel, and the right is the blue channel. (b) The degraded color Lena image. Spatial degradation given by (7.2) is used and the SNR is 20, 30, and 40 dB in the red, green, and blue channels, respectively. Left: red channel, middle: green channel, and right: blue channel. (c) Restored by independent-channel Kalman filter using the original image f to estimate the model. Left: red channel, middle: green channel, and right: blue channel. (*Continued on next page.*)

128×128 skiers image was used. First, the three channels were degraded by the degradation $\tilde{H}$ given by (7.5) where $H^{(i,j)}$ are $M^2 \times M^2$ block Toeplitz submatrices representing low-pass blurring filters implemented as convolution masks. The submatrices $H^{(R,R)}$, $H^{(R,G)}$, and $H^{(R,B)}$ were implemented as 1×5 convolution operators with $1/5$ weights; $H^{(G,R)}$, $H^{(G,G)}$, and $H^{(G,R)}$ were 5×1 masks with $1/5$ weights; $H^{(B,R)}$, $H^{(B,G)}$, and $H^{(B,B)}$ were

(d)

(e)

(f)

Fig. 2. (*Continued.*) (d) Restored by multichannel Kalman filter using the original image f to estimate the model. Left: red channel, middle: green channel, and right: blue channel. (e) Restored by independent-channel Kalman filter using the degraded image g to estimate the model. Left: red channel, middle: green channel, and right: blue channel. (f) Restored by multichannel Kalman filter using the degraded image g to estimate the model. Left: red channel, middle: green channel, and right: blue channel. (*Continued on next page.*)

5×5 masks with $1/25$ weights. A full degradation $\tilde{H}$ with between-channel components as in (7.5) was used in one experiment. In another experiment the same degradation but with no between-channel components as in (7.2) was used. White Gaussian noise was added in both cases, resulting in 20-dB SNR in all channels. The MSE

(g)

(h)

Fig. 2. (*Continued.*) (g) Restored by multichannel Kalman filter in the YIQ domain using an image model that contains no between-channel coefficients. The original image f is used to estimate the model. Left: red channel, middle: green channel, and right: blue channel. (h) Restored by multichannel Kalman filter in the YIQ domain using a full image model with between-channel coefficients. The original image f is used to estimate the model. Left: red channel, middle: green channel, and right: blue channel.

TABLE VI
EXPERIMENT THREE: MULTICHANNEL KALMAN RESTORATION OF THE COLOR LENA 128 × 128 IMAGE. THE IMAGE IS DEGRADED BY BOTH SPATIAL AND BETWEEN-CHANNEL BLUR GIVEN BY (7.5). TABLES VI AND VII ARE THE RESTORATION RESULTS OF THE 20 AND 30 dB IMAGES, RESPECTIVELY

	Mean-Square Error (Percentage Improvement%)		
	Channel R	Channel G	Channel B
Without restoration	8.28 (0%)	12.08 (0%)	7.47 (0%)
(i) Independent-channel restoration.	7.26 (12%)	9.66 (20%)	7.13 (5%)
(ii) Multichannel restoration without between-channel model coefficients.	4.11 (50%)	5.66 (53%)	4.28 (43%)
(iii) Multichannel restoration with between-channel model coefficients.	3.97 (52%)	5.35 (56%)	4.18 (44%)

The results of the experiments are: (i) Independent-channel restoration. (ii) Multichannel restoration, neglecting the between-channel coefficients in the image model. (iii) Multichannel restoration, using the between-channel coefficients in the image model. The image model in all cases is estimated using the original image f.

TABLE VII
SAME AS TABLE VI, EXCEPT SNR = 30 dB

	Mean-Square Error (Percentage Improvement%)		
	Channel R	Channel G	Channel B
Without restoration	8.08 (0%)	11.79(0%)	7.30 (0%)
(i) Independent-channel restoration.	6.52 (19%)	8.45 (28%)	6.76 (7%)
(ii) Multichannel restoration without between-channel model coefficients.	3.89 (52%)	4.91 (58%)	3.93 (46%)
(iii) Multichannel restoration with between-channel model coefficients.	3.08 (62%)	3.58 (70%)	3.07 (58%)

results from this experiment are tabulated in Tables VIII and IX. The findings of this experiment agreed with previous results.

VIII. CONCLUSIONS

Multichannel imagery consists of channels that are interelated. The two most important elements of between-

(a)

(b)

(c)

Fig. 3. (a) The degraded color Lena image. Both spatial and between-channel degradation given by (7.5) were used and the SNR is 30 dB in all channels. Left: red channel, middle: green channel, and right: blue channel. (b) Restored color Lena image by independent-channel Kalman filter, where no between-channel degradation can be used. Left: red channel, middle: green channel, and right: blue channel. Note the ringing artifacts. (c) Restored color Lena image by multichannel Kalman filter using an image model that contains no between-channel coefficients. Left: red channel, middle: green channel, and right: blue channel. (*Continued on next page.*)

channel information for multichannel image restoration are between-channel degradation and between-channel correlation. Restoration using traditional single-channel Kalman filters can incorporate neither one.

Multichannel Kalman filtering has been formulated to incorporate between-channel correlation for the restoration of both spatial and between-channel blur. Moreover, a computational filter for the Kalman formulation has been developed. For an $M \times M$ N-channel image with blurring length Λ, the computational complexity of the Kalman fil-

(d)

Fig. 3. (*Continued.*) (d) Restored color Lena image by multichannel Kalman filter using a full image model that contains between-channel coefficients. Left: red channel, middle: green channel, and right: blue channel.

TABLE VIII
EXPERIMENT FOUR: MULTICHANNEL KALMAN FILTER RESTORATION OF THE COLOR SKIERS IMAGE DEGRADED BY BOTH SPATIAL AND BETWEEN-CHANNEL BLUR GIVEN IN (7.5) AND ADDITIVE NOISE. THE SNR OF ALL THREE CHANNELS WAS 20 dB

		Mean-Square Error (Percentage Improvement%)		
		Channel R	Channel G	Channel B
	Without restoration	12.42 (0%)	13.11 (0%)	17.11 (0%)
(i)	Independent Kalman filter	9.86 (20%)	11.09 (15%)	13.98 (18%)
(ii)	Multichannel Kalman filter without between-channel coefficients	9.62 (23%)	10.11 (23%)	10.82 (36%)
(iii)	Multichannel Kalman filter with between-channel coefficients	7.85 (37%)	8.09 (38%)	8.74 (49%)

The results of the experiments are: (i) Independent-channel Kalman filter restoration, that is, the between-channel blur and between-channel image correlation are not used. (ii) Multichannel Kalman filter restoration using between-channel blur but not between-channel image correlation. (iii) Multichannel Kalman filter restoration using both between-channel blur and between-channel image correlation.

TABLE IX
EXPERIMENT FOUR: MULTICHANNEL KALMAN FILTER RESTORATION OF THE COLOR SKIERS IMAGE DEGRADED ONLY BY SPATIAL BLUR AND ADDITIVE NOISE. THE SNR OF ALL THREE CHANNELS WAS 20 dB

		Mean-Square Error (Percentage Improvement%)		
		Channel R	Channel G	Channel B
	Without restoration	11.27 (0%)	12.57 (0%)	12.63 (20%)
(i)	Independent Kalman filter	8.39 (25%)	10.50 (16%)	12.63 (20%)
(ii)	Multichannel Kalman filter Stationary model	6.60 (41%)	7.96 (36%)	8.36 (47%)
(iii)	Multichannel Kalman filter Nonstationary model	6.52 (42%)	7.82 (38%)	8.30 (48%)

The results of the experiments are: (i) Independent Kalman filter restoration, the between-channel image model coefficients are assumed to be zero. (ii) Multichannel Kalman filter restoration using between-channel coefficients and the stationary model. (iii) Multichannel Kalman filter restoration using between-channel coefficients and the nonstationary model.

ter is reduced from $O(\Lambda^3 N^3 M^4)$—the requirement for $O(M)$ multiplications of $\Lambda NM \times MN\Lambda$ full matrices, to $O(\Lambda^3 N^3 M^2)$—the requirement for $O(M)$ multiplications of $\Lambda NM \times MN\Lambda$ form-D matrices. For $128 \times 128 \times 3$ images with blurring length $\Lambda = 5$, this amounts to a reduction from $O(10^{10})$ to $O(10^6)$.

Experiments were performed to test the proposed filter and the following summarizes our observations: a) Between-channel degradation is essential for accurate restoration of multichannel images. Using color RGB images, it was shown that the proposed filter effectively restored between-channel blur. b) Multichannel imagery

which exhibits strong between-channel correlation greatly benefits from multichannel processing because between-channel coefficients are used in the image models. On the contrary, multichannel imagery with weak between-channel correlations does not benefit from multichannel image models. Color images in the RGB domain were used as an example of multichannel images with strong between-channel correlation. Color images in the YIQ domain were used as an example with weak between-channel correlations. c) Stationary and nonstationary image models were developed and tested. The nonstationary image model only yields a slight improvement over the stationary model; the additional computation does not justify the achieved improvement.

Finally, it is noted that the multichannel Kalman filter is comparable to the multichannel Wiener filter [5] and [6], when the same amount of prior information is available. Both filters assume the knowledge of the additive noise and multichannel degradation. However, the Kalman filter offers the flexibility of processing spatially varying images at the cost of a complex implementation. The problem of simultaneous estimation of degradation and restoration for multichannel images remains to be investigated.

Acknowledgment

The authors would like to acknowledge the help of the anonymous reviewers. Their comments greatly improved the clarity of this paper.

References

[1] H. C. Andrews and B. R. Hunt, *Digital Image Restoration*. Englewood Cliffs, NJ: Prentice-Hall, 1977.

[2] J. Bescos, I. Glaser, and A. A. Sawchuk, "Restoration of color images degraded by chromatic aberration," *Appl. Opt.*, vol. 19, pp. 3869-3876, 1980.

[3] J. Biemond, J. J. Rieske, and J. J. Gerbrands, "A fast Kalman filter for images degraded by both blur and noise," *IEEE Trans. Acoust., Speech, Signal Processing*, vol. 31, no. 5, pp. 1248-1256, Oct. 1983.

[4] J. Biemond, F. G. van der Putten, and J. Woods, "Identification and restoration of images with symmetric noncausal blurs," *IEEE Trans. Circuits Syst.*, vol. 23, no. 3, pp. 385-394, 1988.

[5] N. P. Galatsanos, "Multichannel image restoration," Ph.D. dissertation, Univ. of Wisconsin-Madison, Aug. 1989.

[6] N. P. Galatsanos and R. T. Chin, "Digital restoration of multichannel images," *IEEE Trans. Acoust., Speech, Signal Processing*, vol. 37, no. 3, pp. 415-421, Mar. 1989.

[7] D. Ghiglia, "Space-invariant deblurring given N independently blurred images of a common object," *J. Opt. Soc. Amer. A*, vol. 1, no. 4, pp. 398-402, Apr. 1982.

[8] B. R. Hunt and O. Kübler, "Karhunen-Loeve multispectral image restoration, part I: Theory," *IEEE Trans. Acoust., Speech, Signal Processing*, vol. 32, pp. 592-599, June 1984.

[9] A. K. Jain, "Advances in mathematical models for image processing," *Proc. IEEE*, vol. 69, pp. 502-528, May 1981.

[10] A. K. Katsaggelos, "A multiple input image restoration algorithm," *J. Visual Commun. Image Processing*, pp. 93-103, Sept. 1990.

[11] R. L. Lagendijk, A. M. Tekalp, and J. Biemond, "Maximum likelihood image and blur identification: A unifying approach," *Opt. Eng.*, vol. 29, no. 5, pp. 422-435, May 1990.

[12] K. T. Lay and A. K. Katsaggelos, "Image identification and restoration based on the expectation-maximization algorithm," *Opt. Eng.*, vol. 29, no. 5, pp. 436-445, May 1990.

[13] P. Meer, J. Jolion, and A. Rosenfeld, "A fast parallel algorithm for blind estimation of noise variance," *IEEE Trans. Pattern Analysis Mach. Intell.*, vol. 12, no. 2, pp. 216-222, Feb. 1990.

[14] N. Ohyama, M. Yachida, E. Badique, J. Tsujiuchi, and T. Honda, "Least squares filter for color-image restoration," *J. Opt. Soc. Amer. A*, vol. 5, no. 1, pp. 19-24, Jan. 1988.

[15] A. P. Sage and J. L. Melsa, *Estimation Theory with Applications to Communications and Control*. New York: McGraw-Hill, 1971.

[16] W. K. Pratt, "Spatial transform coding of color images," *IEEE Trans. Commun.*, vol. 19, pp. 980-982, 1971.

[17] A. M. Tekalp, H. Kaufman, and J. W. Woods, "Identification of image and blur parameters for the restoration of noncausal blurs," *IEEE Trans. Acoust., Speech, Signal Processing*, vol. 34, pp. 963-972, 1986.

[18] A. M. Tekalp and G. Pavlovic, "Multichannel image modeling and Kalman filtering for multispectral image restoration," *Signal Processing*, vol. 19, no. 3, pp. 221-232, Mar. 1990.

[19] H. J. Trussell, "*A priori* knowledge in algebraic reconstruction methods," in *Advances in Computer Vision and Image Processing*, vol. 1, *Image Reconstruction from Incomplete Observations*, T. S. Huang, Ed. JAI Press, 1984, pp. 265-316.

[20] J. W. Woods and V. K. Ingle, "Kalman filtering in two dimensions: Further results," *IEEE Trans. Acoust., Speech, Signal Processing*, vol. 29, no. 2, pp. 188-197, Apr. 1981.

[21] J. W. Woods and C. H. Radewan, "Kalman filtering in two dimensions," *IEEE Trans. Inform. Theory*, vol. 23, no. 4, pp. 557-566, July 1977.

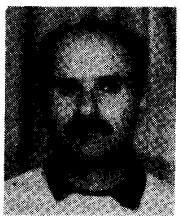

Nikolas P. Galatsanos (S'84-M'85) was born in Athens, Greece, in 1958. He received the Diploma degree in electrical engineering from the National Technical University of Athens, Athens, Greece, in 1982, the M.S. and Ph.D. degrees, both in electrical engineering, from the University of Wisconsin-Madison, in 1984 and 1989, respectively.

Since August 1989, he has been on the faculty of the Department of Electrical and Computer Engineering, Illinois Institute of Technology, Chicago, IL, where he is currently Assistant Professor. His current research interests include image restoration/reconstruction, image coding, and VLSI architectures for signal processing algorithms.

Dr. Galatsanos is a member of the SPIE, OSA, and the Technical Chamber of Greece.

Roland T. Chin (S'75-M'79) received the B.S. degree with honors in 1975 and the Ph.D. degree in 1979 in electrical engineering from the University of Missouri, Columbia.

From 1979 to 1981, he was with Business and Technological Systems, Inc., Maryland, where he engaged in research in remote sensing data analysis and classification for NASA Goddard Space Flight Center, Greenbelt, MD. Since 1981, he has been on the faculty of the Department of Electrical and Computer Engineering, University of Wisconsin-Madison, where he is currently a Professor. His current research interests include image restoration, texture analysis, shape descriptions, pattern recognition, visual inspection, object recognition, and related applications.

Dr. Chin is a member of Eta Kappa Nu and Tau Beta Pi and he was the recipient of the 1984 Presidential Young Investigator Award.